TOPICAL REVIEW

Magnetic refrigerants for ultralow temperatures: A mini-review

TOPICAL REVIEW — Multiferroicity and multicaloric effects

Magnetic refrigerants for ultralow temperatures: A mini-review

Ziyu W. Yang(杨子煜)[1,3], Shuai Tang(唐帅)[1,2], Guangkai Zhang(张广凯)[1], Ciyu Qin(秦慈宇)[1,2], Maocai Pi(皮茂材)[1,2], Xubin Ye(叶旭斌)[1], Zhao Pan(潘昭)[1], Yu-Jia Zeng(曾昱嘉)[3], and Youwen Long(龙有文)[1,2,†]

[1] *Beijing National Laboratory for Condensed Matter Physics, Institute of Physics, Chinese Academy of Sciences, Beijing* 100190, *China*
[2] *School of Physical Sciences, University of Chinese Academy of Sciences, Beijing* 100049, *China*
[3] *Key Laboratory of Optoelectronic Devices and Systems of Ministry of Education and Guangdong Province, College of Physics and Optoelectronic Engineering, Shenzhen University, Shenzhen* 518060, *China*

(Received 14 November 2025; revised manuscript received 26 November 2025; accepted manuscript online 27 November 2025)

Accessing the milli-Kelvin regime is increasingly important for next-generation quantum technologies and deep-space observations. Among established cryogenic techniques, adiabatic demagnetization refrigeration (ADR) is distinctive for its all-solid-state design, low vibration, and intrinsic gravity independence. Here we present a materials-centered review of ADR refrigerants, connecting classical thermodynamics to modern quantum many-body behavior. Beyond hydrated paramagnetic salts, dense rare-earth oxides and correlated-disorder ceramics, we highlight emerging quantum-engineered refrigerants, including geometrically frustrated magnets, and quantum-critical systems. In these materials, suppressing long-range order and tailoring low-energy excitations redistribute spin entropy into the sub-Kelvin window, enabling large and reversible entropy changes at the lowest accessible temperatures. We discuss the central trade-offs among volumetric entropy density, thermal transport, and magnetic ordering, and outline possible design rules for staged ADR architectures.

Keywords: adiabatic demagnetization refrigeration, magnetocaloric effect, cryogenics

PACS: 07.20.Mc, 75.30.Sg, 71.27.+a

DOI: 10.1088/1674-1056/ae24f0 **CSTR:** 32038.14.CPB.ae24f0

1. Introduction

The ultralow temperature regime (typically below 1 K) represents an important frontier in modern physics and advanced technology. At these temperatures, thermal noise is greatly reduced, allowing macroscopic quantum phenomena to appear clearly, such as superconductivity, superfluidity and possible supersolid-like phases, revealing complex many-body energy landscapes. This environment is ideal for high-sensitivity detection methods (including x-ray spectroscopy, far-infrared sensing, and dark matter searches) as well as groundbreaking innovations like quantum computing.[1–4] Currently, the main cooling methods for reaching ultralow temperatures include ^{3}He evaporative refrigeration (reaching ~ 0.3 K), ^{3}He–^{4}He dilution refrigeration, and adiabatic demagnetization refrigeration (ADR).

Among these, dilution refrigerators can operate continuously down to the milli-Kelvin regime (typically reaching base temperatures < 10 mK), while offering a moderate cooling power. However, they face practical limitations, such as structural complexity, reliance on ^{3}He circulation, and mechanical vibration. Furthermore, conventional wet dilution refrigerators rely on gravity-assisted phase separation, making them difficult to adapt for space missions without complex modifications (such as open-cycle dilution or closed-cycle sorption systems).[5]

In contrast, ADR is inherently gravity-independent. It offers a simpler, fully solid-state architecture that avoids the complexities of gas handling and fluid circulation, making it particularly attractive for achieving deep cryogenic environments in space. At $T < 1$ K, the volumetric cooling power and efficiency of ADR can be competitive for certain mission constraints to those of dilution refrigeration. Furthermore, its flexible design allows for single-stage, multi-stage cascaded or continuous cycling operations.

The principle of ADR was independently proposed by Debye and Giauque in 1926 to 1927, and was experimentally demonstrated seven years later by Giauque and MacDougall (1933).[6–8] By implementing the adiabatic demagnetization of paramagnetic salts $Gd_2(SO_4)_3{\cdot}8H_2O$, they successfully achieved 0.53 K from a starting temperature of 3.4 K, surpassing the 0.83 K limit of liquid helium evaporation cooling set by Onnes in 1922.[9] Shortly thereafter, de Haas, Wiersma and Kramers employed the technique to reach 0.08 K via demagnetization of cerium ethylsulfate, inaugurating the era of milli-Kelvin physics.[10]

In 1954, Heer, Barnes, and Daunt constructed a device using superconducting thermal switches combined with a high heat capacity reservoir.[11,12] Their device successfully maintained a temperature of 0.26 K under a heat load of 7 μW using $FeNH_4(SO_4)_2{\cdot}12H_2O$. This design was subsequently refined by Zimmerman, McNutt, and Bohm, who incorporated

†Corresponding author. E-mail: ywlong@iphy.ac.cn

superconducting solenoids to achieve a significantly higher heat load of 100 μW.[13] Later, Rosenblum, Sheinberg and Steyert reported a similar refrigerator that pushed the boundaries to the milli-Kelvin regime (base 10 mK under load of 0.1 μW).[14] They utilized the demagnetization of a composite cylinder of gold-cerous magnesium nitrate, and a cobalt metal thermal reservoir, which acts to smooth out the cyclical temperature swings.

The development history of ADR shows its core advantages, such as all-solid-state operation, high reliability, and gravity-independent performance. However, this history also shows a consistent pattern: the performance of ADR systems depends fundamentally on the properties of magnetic refrigerants. From the early paramagnetic salts used by Giauque to the composite materials in Rosenblum's milli-Kelvin refrigerator, each advance in cooling capacity and temperature range has been made possible by improvements in refrigerant design. As cryogenic applications have grown from basic physics laboratories into space missions, x-ray astronomy, and quantum computing, the demands on ADR refrigerants have become more challenging. Modern applications require higher magnetic entropy density, wider operational temperature ranges, and carefully controlled magnetic ordering behavior. Therefore, the search for and development of better magnetic refrigerants has become a central task in advancing ADR technology to new levels.

While many excellent reviews on ADR already exist, most focus on the cooling principles, cryogenic engineering, or specific instruments, and only briefly mention the underlying refrigerant materials.[2,15–17] A systematic, materials-centered comparison across both classical and emerging ADR refrigerants is still missing. In this context, we present a short review on ADR refrigerant materials. We begin by introducing key thermodynamic measures for evaluating refrigerant performance. The discussion then moves from classical hydrated paramagnetic salts to structurally disordered compounds, and finally to exotic quantum many-body systems including geometrically frustrated magnets, quantum critical materials, and heavy fermion compounds. For each category, we examine their performance strengths and fundamental challenges in ADR applications. Finally, we provide an outlook on future research directions and the practical potential of advanced ADR technology.

2. Key performance metrics for magnetic refrigerants

Magnetic entropy change $\Delta S(T,B)$ The entropy change at temperature T upon increasing the external field from 0 to B_i is given by the Maxwell relation

$$\Delta S(T,B_\mathrm{i}) = S(T,B_\mathrm{i}) - S(T,0) = \int_0^{B_\mathrm{i}} \left(\frac{\partial M}{\partial T}\right)_B \mathrm{d}B \qquad (1)$$

or calculated from the entropy by integrating of the heat capacity C_p via

$$S(T,B_\mathrm{i}) = S(0,B_\mathrm{i}) + \int_0^T \left(\frac{C_\mathrm{p}(T',B_\mathrm{i})}{T'}\right) \mathrm{d}T'. \qquad (2)$$

Along the isothermal magnetization path $A \to B$ (Fig. 1), the heat Q_m released to the thermal reservoir is

$$Q_\mathrm{m}(T_\mathrm{i},B_\mathrm{i}) = -T_\mathrm{i}\Delta S(T_\mathrm{i},B_\mathrm{i}), \qquad (3)$$

corresponding to the rectangular area *ABCDE* in Fig. 1. Q_m is modest and can be readily absorbed by an evaporating helium bath in typical ADR precooling stages.

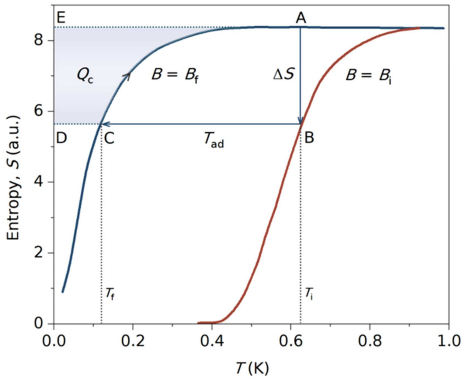

Fig. 1. The S–T diagram for a typical magnetic refrigerant. $A \to B$: isothermal magnetization at T_i from 0 to B_i, releasing heat of magnetization $Q_\mathrm{m} = -T_\mathrm{i}\Delta S(T_\mathrm{i},B_\mathrm{i})$ (area of rectangle *ABCDE*). $B \to C$: adiabatic demagnetization to B_f with $T_\mathrm{ad} = T_\mathrm{i} - T_\mathrm{f}$ set by $S(T_\mathrm{i},B_\mathrm{i}) = S(T_\mathrm{f},B_\mathrm{f})$. $C \to A$: isofield warm-up at B_f; the shaded area represents the available cooling load Q_c.

A large ΔS typically correlates with large spin multiplicity and high magnetic moment density. The maximum available entropy for an ideal paramagnet is $R\ln(2J+1)$, where R is the gas constant and J is the total angular momentum quantum number. However, ΔS alone represents only a stock of available entropy (i.e., an equilibrium thermodynamic quantity), it does not specify the field distribution of this entropy or its accessibility within a given thermodynamic cycle. Therefore, ΔS serves as a useful first-pass screening metric but not as a sufficient performance criterion.

Adiabatic temperature change T_ad The adiabatic demagnetization step $B \to C$ conserves entropy, $S(T_\mathrm{i},B_\mathrm{i}) = S(T_\mathrm{f},B_\mathrm{f})$, defining the adiabatic temperature change T_ad, as $T_\mathrm{ad} = T_\mathrm{i} - T_\mathrm{f}$. In real materials, T_f seldom reaches zero even by letting $B_\mathrm{f} \to 0$, because internal interactions will eventually align the moments and quench the entropy. Typically, for ideal paramagnets or systems far from critical points (assuming $B_\mathrm{i} \gg b$), the final temperature T_f can be estimated as

$$T_\mathrm{f} = \frac{T_\mathrm{i}}{B_\mathrm{i}}\sqrt{B_\mathrm{f}^2 + b^2}, \qquad (4)$$

where b represents the internal field. It is important to note that, for refrigerants whose entropy–temperature relation deviates from simple paramagnetic behavior, T_f is determined by

the specific density of states and the release of residual entropy at zero-field, rather than by a simple effective internal field.

Heat capacity C_p and cooling capacity The heat capacity C_p determines the usable cooling capacity during the heat absorption stage. From the entropy curve ($C \to A$ in Fig. 1), the heat absorbed by the refrigerant during warming from T_f back to T_i at fixed B_f is

$$Q_c(B_f; T_f \to T_i) = \int_{T_f}^{T_i} T \left(\frac{\partial S}{\partial T} \right)_{B_f} \mathrm{d}T, \tag{5}$$

of which the thermodynamic identity $(\frac{\partial S}{\partial T})_B = \frac{C_p(T,B)}{T}$.

The position and magnitude of the low-temperature heat capacity peak determine the fundamental cooling limit of adiabatic demagnetization. Once the temperature approaches the energy scale defined by internal interactions, residual magnetic entropy becomes trapped below the C_p maximum and further cooling stops. The magnitude and width of C_p thus control the thermal buffering capacity: a larger, broader C_p peak in the working temperature range (typically 0.05–1 K) produces smaller temperature rises for a given heat load and longer hold times t. This can be roughly estimated by a time evolution equation under a given P (P represents the total parasitic heat load or external heating power applied to the system) as

$$\frac{\mathrm{d}U[T(t)]}{\mathrm{d}t} = P, \tag{6}$$

where $U(T)$ denotes the internal energy, obtained by integrating C_p.

It must be noted that cycle-averaged cooling power depends additionally on heat-exchange rate and achievable cycle frequency. Therefore, direct measurements of T_{ad} and Q_c under operating conditions provide the most reliable performance benchmarks, beyond ΔS and C_p inferred from equilibrium data. This can be accomplished through two primary approaches: (i) testing in a commercial working ADR system, which provides real operational metrics including hold time, base temperature stability, and cycling performance under actual heat loads; or (ii) laboratory-scale quasi-adiabatic demagnetization measurements, which are more accessible and widely used for rapid materials screening. In the latter approach, the sample is thermally anchored to a heat sink (typically at 2–4 K) under an applied magnetic field, then thermally isolated before field ramping. Temperature evolution during demagnetization is monitored using calibrated cryogenic thermometers (such as CERNOX or ruthenium oxide sensors) in commercial superconducting magnet systems (e.g., physical property measurement system, PPMS). While this method cannot fully replicate the continuous ADR operation (lacking active thermal switching and multistage heat management), it effectively captures the intrinsic magnetocaloric response (T vs. B profiles) and allows direct comparison of candidate refrigerants under standardized conditions. Key experimental considerations include minimizing parasitic heat leaks through support structures, ensuring adequate thermal equilibration time between the sample and thermometer, and accounting for eddy-current heating during field ramping in metallic samples.

Thermal conductivity κ Thermal conductivity κ determines how rapidly Q_m is expelled to the heat sink during stage $A \to B$, and how quickly the load reaches equilibrium with the refrigerant during stages $B \to C$ and $C \to A$. Low κ creates internal temperature gradients, slows cycle rates, and shortens holding time. This limitation is a major weakness of many hydrated paramagnetic salts. In contrast, dense oxides and intermetallic compounds typically show much better heat exchange, typically orders of magnitude higher than hydrated salts, which greatly simplifies cold-finger design, though sometimes at the cost of limited achievable temperatures. Representative single-crystal κ values of $Gd_3Ga_5O_{12}$ (a benchmark refrigerant) are approximately 10^1 $W \cdot m^{-1} \cdot K^{-1}$ at 4 K and 10^2 $W \cdot m^{-1} \cdot K^{-1}$ at 10 K.[18]

Chemical and mechanical robustness ADR refrigerants must withstand high vacuum and repeated cryogenic cycling. For space applications, radiation tolerance is also essential. Classical hydrated salts are sensitive to environmental humidity, easily losing water or deliquescing, which leads to performance degradation. Dense ceramics or intermetallic compounds offer more robust packaging and stable long-term operation. Therefore, new refrigerants often prioritize chemically inert, mechanically strong material forms to ensure stable performance in practical applications.

3. Magnetic refrigerant materials

3.1. Hydrated paramagnetic salt

Paramagnetic salts containing ions with partially filled electronic shells, such as 3d transition metal ions and 4f rare earth ions, were the first refrigerants employed in adiabatic demagnetization cooling. This choice was primarily driven by the material technology available at that time, for which hydrated salts could be readily synthesized as large, high-purity single crystals from aqueous solutions, making them experimentally accessible. In these compounds, the crystallization water molecules separate magnetic ions from each other, thus weakening magnetic dipolar and exchange interactions. This reduces the magnetic energy scale to the milli-Kelvin range, thereby delaying spontaneous magnetic ordering to ultralow temperatures.

Alum salts (manganous ammonium sulfate MAS: $Mn(NH_4)_2(SO_4)_2 \cdot 6H_2O$; ferric ammonium alum FAA: $FeNH_4(SO_4)_2 \cdot 12H_2O$; chromium potassium alum CPA:

$KCr(SO_4)_2{\cdot}12H_2O$): Containing 3d transition metal magnetic ions with quenched orbital angular momentum ($g \approx 2$), magnetic moments are primarily from spin, such as Mn^{2+} ($S = 5/2$), Fe^{3+} ($S = 5/2$), Cr^{3+} ($S = 3/2$). Typical zero-field magnetic ordering temperatures: MAS $\sim$ 170 mK, FAA $\sim$ 30 mK, CPA $\sim$ 10 mK.[19,20]

Cerium magnesium nitrate (CMN, $Ce_2Mg_3(NO_3)_{12}{\cdot}24H_2O$): Below $T \approx 1$ K, its crystal field ground state is an effective $J = 1/2$ doublet, with paramagnetic behavior persisting down to $\sim$ 6 mK. The La-doped dilution can go even lower, though at the cost of reducing volumetric entropy capacity. The spontaneous magnetic ordering temperature under zero field of CMN is among the lowest reported for electronic paramagnetic salts.[19]

In practice, the extremely low thermal conductivity of hydrated salts at cryogenic temperatures requires embedding them in a metal wire mesh to improve heat conduction. Without these measures, temperature gradients easily form during demagnetization, making low temperatures difficult to maintain. Additionally, these salts are sensitive to humidity, requiring careful attention to sample preparation and packaging.

3.2. Dense rare-earth compounds

Although hydrated salts still hold records for extremely low temperatures, the emergence of new dense magnetic materials has opened more application possibilities for ADR. These materials, as complementary solutions, cover the intermediate temperature range of 1–4 K with their higher thermal conductivity and mechanical strength, significantly enhancing the overall volumetric cooling power.

Gadolinium gallium garnet ($Gd_3Ga_5O_{12}$, GGG) is a typical example. The Gd^{3+} ion density reaches 12.6 nm^{-3}, with ground-state volumetric magnetic entropy of 363 $mJ{\cdot}K^{-1}{\cdot}cm^{-3}$.[22] More importantly, GGG does not show long-range order until < 20 mK in zero field, meaning it maintains high magnetic entropy and reversible magnetic cycling in the liquid helium temperature range when most strong magnets have ordered (Fig. 2).[21] Furthermore, GGG can be grown as large single crystals, with thermal conductivity of 40 $W{\cdot}m^{-1}{\cdot}K^{-1}$ at 4 K, orders of magnitude higher than hydrated salts, thus allowing direct processing without complex thermal connections.[18] Modern multi-stage ADR often uses GGG as the first stage, precooling hydrated salts at 0.8–2 K before demagnetizing to < 0.2 K.

The garnet structure also offers considerable flexibility for tuning magnetic properties through rare-earth substitution. Replacing Gd^{3+} in GGG with other rare-earth ions, such as Tb^{3+}, Dy^{3+}, or Yb^{3+} to form $Tb_3Ga_5O_{12}$, $Dy_3Ga_5O_{12}$, and $Yb_3Ga_5O_{12}$, systematically adjusts the magnetic ordering temperature, crystal-field splitting, and effective magnetic moment.[21,23] These variations enable materials optimization for specific temperature regimes. Beyond simple rare-earth substitution, partial replacement of Ga^{3+} by magnetic Fe^{3+} ions in gadolinium gallium iron garnet (GGIG, $Gd_3(Ga_{1-x}Fe_x)_5O_{12}$) introduces additional magnetic interactions, allowing fine-tuning of the magnetic entropy profile and ordering temperature through composition control.[24]

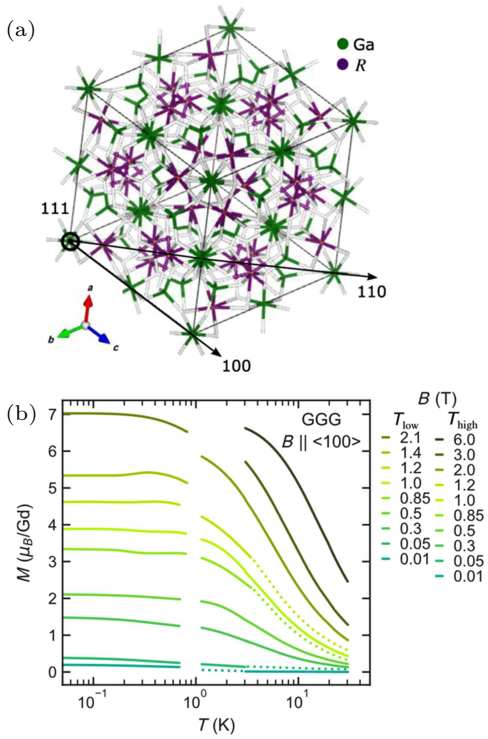

Fig. 2. (a) Crystallographic structure of $R_3Ga_5O_{12}$, R = rare earths, along the $\langle 111 \rangle$ axis. (b) Magnetization of $Gd_3Ga_5O_{12}$ single crystal as a function of temperature and applied fields parallel to $\langle 100 \rangle$ direction. Reproduced with permission from Ref. [21].

Gadolinium lithium fluoride (GLF, $GdLiF_4$) possesses large $S = 7/2$ magnetic moments, with magnetic ordering temperature < 0.3 K and isothermal entropy change 20%–60% higher than GGG, now manufacturable as large single crystals.[25,26] GdF_3 also provides considerable entropy capacity and thermal conductivity in the 0.3–1 K range.[27]

Common features of these materials include high entropy change from high magnetic ion density and large magnetic moments; low ordering temperature ensured by frustrated or weakly coupled magnetic interactions; high thermal conductivity and chemical stability endowed by dense crystal structure. They serve as complementary refrigerants to hydrated salts, facilitating efficient ADR operation across the extended 0.05–4 K temperature window. Notably, considerable research efforts in magnetic refrigerants have focused on this temperature regime, with numerous studies exploring alternative Gd^{3+}- and Eu^{2+}-based materials that aim to surpass the benchmark GGG series.[28–43]

3.3. Structurally disordered magnetic refrigerants

Beyond the classical hydrated salts characterized by weakly interacting ordered lattices, structural disorder offers

an alternative and promising avenue for ADR refrigerant design. Structural disorder encompasses various lattice imperfections, including site mixing, random distortions of bond lengths and angles, vacancies, and stacking faults. These structural features randomize the exchange interaction distribution between magnetic ions and reduce the effective connectivity of the spin network. Consequently, long-range magnetic ordering is suppressed to temperatures far below the Curie–Weiss temperature. Macroscopically, this suppression manifests as the absence of a sharp magnetic phase transition. Instead, the system exhibits a broad distribution of short-range magnetic correlations and low-energy excitations, which are particularly advantageous for ADR applications.

We demonstrate how correlated disorder enhances cooling performance in $Gd_{9.33}[SiO_4]_6O_2$, a rare-earth oxyapatite-type silicate featuring highly correlated occupancy disorder.[44] The stochastic interruption of Gd^{3+} occupancy by vacancies disrupts three-dimensional magnetic connectivity, suppressing long-range magnetic order down to 50 mK (Fig. 3). This correlated disorder induces distributed modifications to exchange pathways and local magnetic environments, giving rise to a spin-liquid like disordered ground state. Experimental results reveal exceptional cooling performance in the sub-Kelvin regime, characterized by large reversible magnetic entropy changes and significant adiabatic temperature changes. Critically, the magnetocaloric effect is among the highest ever reported, and extends across a broad temperature range rather than being confined to a discrete phase transition point.

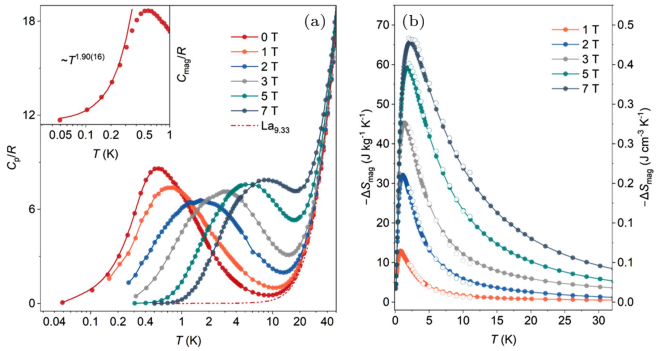

Fig. 3. (a) Heat capacity C_p of $Gd_{9.33}[SiO_4]_6O_2$ measured down to 50 mK under varying constant applied fields. (b) Magnetic entropy changes as a function of magnetic field and temperature of $Gd_{9.33}[SiO_4]_6O_2$. Reproduced with permission from Ref. [44].

Another typical example is the mixed rare-earth fluoride $LiGd_{0.1}Yb_{0.9}F_4$, which forms a heterogeneous magnetic network through occupational disorder of Yb^{3+} and Gd^{3+} ions, suppressing the magnetic ordering temperature to $\sim$ 85 mK. $LiGd_{0.1}Yb_{0.9}F_4$ exhibits a maximum isothermal magnetic entropy change of $\sim$ 136 mJ·cm^{-3}·K^{-1} at 0.68 K under 2 T, approximately three times that of classical CPA.[45]

From an ADR perspective, carefully designed disorder brings key advantages: (i) lowered magnetic ordering temperature enabling large entropy capacity at 0.05–1 K; (ii) continuous, reversible magnetization process without sharp phase transitions or hysteresis; (iii) broadened magnetocaloric response enabling stable multi-stage operation across extended field and temperature ranges. Disorder creates an "entropy reservoir" in the sub-Kelvin regime by reducing the ordering energy scales and broadening low-energy density of states. External fields progressively rearrange the near-degenerate configurations, thus yielding smooth isentropes with large slopes. Beyond their magnetic advantages, disordered ceramics offer significant practical benefits, the structural strength without crystallization water enables direct machining into complete cooler components without hygroscopic risks.

However, disorder also brings some trade-offs. First, internal random fields and dipolar interactions create an ultralow temperature plateau, limiting the minimum achievable temperature. Second, excessive disorder may cause slow spin dynamics that compromise reversibility (i.e., randomness and frustration lead to non-ergodic behavior below a freezing temperature). Third, enhanced phonon scattering lowers thermal conductivity compared to ordered crystals. Fortunately, these effects can be reduced through geometric optimization, improved thermal interface, or partial substitution with non-magnetic ions.

3.4. Quantum many-body effects enhanced cooling

Traditional paramagnetic refrigerants achieve low ordering temperatures through minimal magnetic interactions, which inevitably limits their magnetic moment density and entropy capacity. Quantum many-body effects offer a way to overcome this fundamental trade-off. Quantum fluctuations and entanglement redistribute entropy into a dense set of low-energy collective excitations, allowing a large fraction of the total spin entropy to remain accessible in the sub-Kelvin range. This enables modern ADR materials to simultaneously achieve disorder at ultra-low temperatures and enhanced cooling capacity. The key is to engineering specific magnetic interaction geometries that strengthen quantum fluctuations while maintaining thermodynamic reversibility.

3.4.1. Geometrically frustrated antiferromagnets

In geometrically frustrated spin systems, such as the 2D triangular and kagome lattices, 3D pyrochlore, garnet and trillium lattices, or confined cluster structures, competing exchange pathways prevent the system from forming a unique long-range order. Instead, the system produces numerous degenerate or near-degenerate low-energy spin configurations. In such a manifold of (quasi-)degenerate low-lying spin states, a large fraction of the spin entropy remains accessible over an extended low-temperature range. Applied magnetic fields can reshuffle the populations of these nearly degener-

ate states, significantly redistributing entropy among the low-lying levels.[46,47] According to the thermodynamic relation

$$\left(\frac{\partial T}{\partial B}\right)_S = -T\frac{(\partial S/\partial B)_T}{C}, \tag{7}$$

if a material has large specific heat C at low temperatures and $(\partial S/\partial B)_T$ is abnormally sensitive to magnetic field changes, then the absolute value of $(\partial T/\partial B)_S$ becomes large, producing strong cooling effects. Importantly, the cooling mechanism in frustrated systems is continuous and reversible, making it suitable for repeated ADR cycling. Moreover, many frustrated compounds are themselves dense solids with high magnetic moment density and good mechanical and chemical stability.

A promising example is the recently reported Eu(II) triangular network coordination polymer $Eu_{0.9}Ba_{0.1}I_2(pyrazine)_3$, which demonstrates excellent sub-Kelvin cooling performance. Eu^{2+} has large $S = 7/2$ magnetic moments and forms a two-dimensional triangular layered structure, with isothermal entropy change as high as 24 $J{\cdot}kg^{-1}{\cdot}K^{-1}$ at 1.4 K and $\Delta B = 7$ T, achieving a significant adiabatic temperature drop in the sub-Kelvin range. Direct demagnetization curves show a plateau near 0.17 K, with the minimum temperature limited by internal dipolar field effects.[48]

Finite-dimensional frustrated Gd^{3+} clusters offer a molecular-scale realization of this cooling mechanism. The compound $[Gd_7(OH)_6(thmeH_2)_5(thmeH)(tpa)_6(MeCN)_2](NO_3)_2$ (denoted as Gd_7) consists of planar hexagonal clusters composed of seven Gd^{3+} ions.[49] These clusters show clear steps in the magnetization curve due to internal geometric frustration. In quasi-adiabatic measurements, demagnetization from an initial temperature of 1 K can reach ~ 0.2 K, corresponding to a pronounced valley in the T–B isentropes at the magnetization plateau (Fig. 4). These discrete clusters directly verify the core principle of frustrated cooling, that highly degenerate ground states combined with magnetic-field-driven reconstruction of the energy spectrum. They also reveal that at ultra-low temperatures, magnetic dipolar interactions introduce internal effective fields that set the base temperature limit.

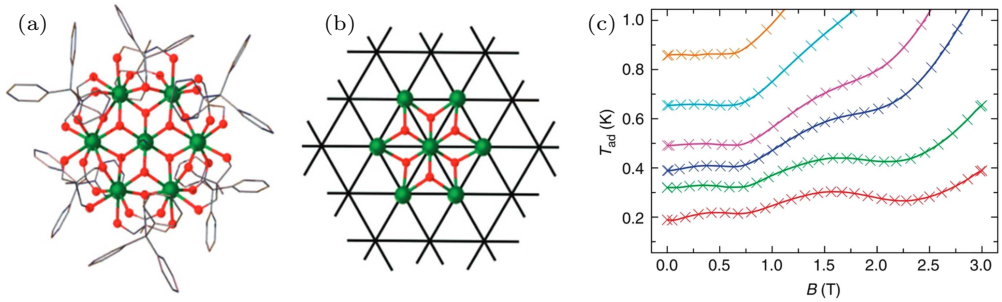

Fig. 4. Crystal structure of frustrated Gd_7 complex (a) and its core mapped onto a triangular spin topology (b). (c) The experimental quasi-adiabatic temperature evolution of Gd_7 complex, with a minimal temperature below 200 mK. Reproduced with permission from Ref. [49].

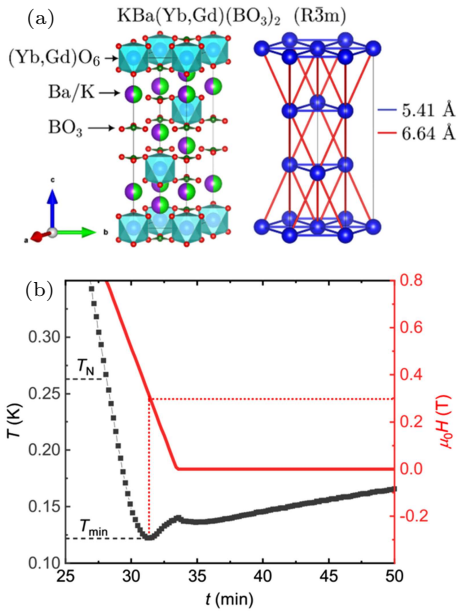

Fig. 5. (a) Crystal structures and lattice geometries of $KBaR(BO_3)_2$, R = rare earths. (b) Quasi-adiabatic demagnetization of triangular $KBaGd(BO_3)_2$ powders. Reproduced with permission from Refs. [16,52].

Extending to three-dimensional coordination frameworks, the trillium molecular compound $Na[Mn(HCOO)_3]$ demonstrates how geometric frustration in the classical spin-liquid regime can be exploited for magnetocaloric applications.[50] Here, frustration suppresses long-range order and enhances fluctuations, enabling switching between ordered and disordered states under low applied fields. This results in a pronounced magnetic entropy change at field-driven transitions. Specifically, the transformation from a spin-liquid state to an up-up-down ordered phase yields a peak ΔS comparable to that of commercial magnetocaloric materials, demonstrating that frustrated magnets can achieve competitive cooling power even in finite-field regimes.

A particularly successful materials platform emerges when geometric frustration is coupled with controlled structural disorder, as exemplified by the layered rare-earth borates $KBaR(BO_3)_2$ (R = rare earths). In $KBaYb(BO_3)_2$, the triangular layer geometry induces geometric frustration, while random cation occupations further suppress magnetic ordering far below the Curie–Weiss temperature.[51] Adiabatic demagnetization from an initial temperature of 2 K under a several-Tesla

field can reach temperatures in the tens of mK range, achieving < 20 mK under optimized conditions, a performance comparable to that of classical paramagnetic salts. The isostructural $KBaGd(BO_3)_2$, despite undergoing a weak ordering transition near 0.25 K, can still be demagnetized to ~ 0.12 K and maintains relatively long hold times at low temperatures (Fig. 5).[52] The robust cooling performance across this family, even in the presence of phase transitions, highlights the practical advantages of frustrated magnetic refrigerants.

3.4.2. Heavy fermion metals and quantum critical magnets

Beyond classical frustrated magnets, heavy fermion systems provide another platform for enhanced adiabatic demagnetization refrigeration through quantum criticality.[53] In these materials, localized f-electron moments hybridize with conduction electrons via Kondo coupling, while Ruderman–Kittel–Kasuya–Yosida (RKKY) exchange mediates indirect magnetic interactions between local moments. The competition between these mechanisms determines the ground-state properties and can be tuned via magnetic field, chemical substitution, or pressure toward a quantum critical point (QCP). Approaching the QCP, both the $C_{\rm el}/T$ (electronic specific heat, $C_{\rm el}$) and the magnetic Grüneisen parameter $\Gamma_{\rm B} = (\partial T/\partial B)_{\rm S}/T$ exhibit power-law or logarithmic divergences, signaling critical enhancement of entropy and field-response.

This thermodynamic amplification near criticality has direct consequences for magnetic cooling. Entropy accumulates and redistributes such that isentropes compress sharply around the critical field $B_{\rm c}$, enabling substantial temperature changes under modest field variations. The resulting scenario provides all essential ingredients for effective ADR: (i) large, field-tunable magnetic entropy persisting below 1 K; (ii) smooth, reversible thermodynamic trajectories in the absence of first-order transitions and hysteresis; and (iii) metallic thermal conductivity ensuring rapid thermal equilibration with the load.

An ADR unit employing the heavy fermion compound $YbCu_4Ni$ achieves demagnetization cooling from 1.8 K to approximately 0.20 K with continuous temperature control.[54] $YbNi_{1.6}Sn$ shows unusually small Kondo and RKKY interactions, which allows the materials to retain high entropy into the 100 mK regime, enabling a base temperature of 116 mK under a 0.4 μW load (Fig. 6).[55] The super-heavy electron alloy $Yb_{0.81}Sc_{0.19}Co_2Zn_{20}$, positioned near a QCP with $C_{\rm el}/T \approx 8.5$ J·mol^{-1}·K^{-2}, cools from 1 K to about 40 mK, with thermal modeling predicting further gains under optimized thermal isolation and magnetic shielding.[56]

Importantly, quantum criticality-enhanced ADR is not limited to metallic compounds. Insulating quantum magnets near field-induced QCP also exhibit this behavior. For instance, the $S = 1/2$ Heisenberg antiferromagnetic chain compounds, Cu-based coordination polymer [Cu(μ-C_2O_4) (4 aminopyridine)$_2$(H_2O)]$_n$), show critical enhancement of the magnetocaloric effect, and enable efficient cooling to approximately 132 mK.[57]

Taken together, these advances demonstrate that quantum criticality extends the operational reach of ADR into the 0.1–0.3 K regime and below, complementing traditional paramagnetic salt stages. It is worth noting that while the divergence of the Grüneisen parameter $\Gamma_{\rm B}$ near the QCP implies a massive differential temperature change, this enhancement is typically confined to a narrow magnetic field range around $B_{\rm c}$. Practical ADR applications require high integral cooling capacity ($\int T\,{\rm d}S$) over the full demagnetization cycle (e.g., 4 T→ 0 T). Therefore, quantum critical materials are best suited for specific temperature control stages requiring high sensitivity, rather than as broad-range bulk heat sinks.

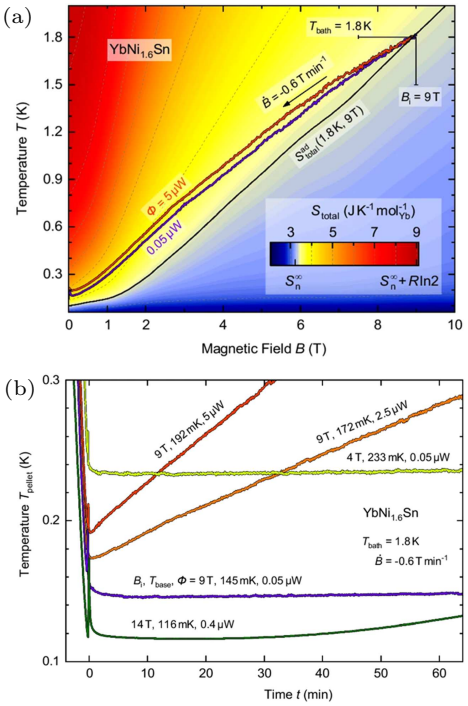

Fig. 6. Demagnetization cooling performance of $YbNi_{1.6}Sn$, with trajectories of temperature vs. field (a) and warming time (b) under varied heat loads. Reproduced with permission from Ref. [55].

4. Conclusion and perspectives

The evolution of ADR refrigerant materials reveals a clear paradigm shift: from classical weakly interacting paramagnetic salts exploiting single-ion entropy toward modern quantum many-body systems harnessing collective phenomena-geometric frustration, quantum criticality, heavy-fermion physics, and correlated disorder to achieve cooling performance beyond the practical limitations of nearly ideal paramagnets. This progression has systematically pushed operational capabilities from the Kelvin regime into the deep sub-Kelvin and milli-Kelvin range, dramatically expanding the reach and efficiency of ADR.

We summarize here the key characteristics of the discussed refrigerant families in Table 1. It is important to emphasize that this classification is somewhat heuristic, as the boundaries between categories are often blurred in modern quantum materials. For instance, a heavy-fermion metal may simultaneously exhibit geometric frustration, and a structurally disordered ceramic can be viewed as a distinct class of frustrated system.

However, from an engineering perspective, these groupings reflect the dominant limiting factors and operational niches: hydrated salts define the traditional limit of base temperature and low thermal conductivity; dense compounds represent the benchmark for volumetric capacity in the intermediate stage; disordered and frustrated systems offer specific solutions to suppress ordering for sub-Kelvin stability; quantum critical metals address the conductivity bottleneck at the cost of introducing possible parasitic eddy currents. By mapping these families against their typical ordering temperatures and entropy densities, Table 1 serves as a quick-reference landscape for selecting materials tailored to specific cooling stages.

Table 1. Classification of magnetic refrigerant families based on their dominant physical mechanisms and engineering characteristics. The values for ordering temperature and operational windows are indicative and may vary for specific compounds. This mapping highlights the trade-offs between entropy capacity, thermal transport, and implementation complexity across different temperature regimes.

Material family	Magnetic ordering temperature (coarse classification)	Volumetric entropy density	Thermal conductivity	Key strengths	Main limitations
Hydrated paramagnetic salts (e.g. MAS, FAA, CPA, CMN)	$\sim$ 10–100 mK	Low (water molecules & loose packing)	Very low (need metal mesh/ wires)	Very high single-ion entropy; record low base temperatures; cheap; easy synthesis.	Chemical instability (dehydration); corrosive, fragile, hygroscopic crystals; poor thermal contact; low volumetric cooling power.
Dense rare-earth compounds (e.g. GGG series, GdF_3, $GdLiF_4$)	0.2–1.5 K	High (compared to paramagnetic salts)	High to low (single crystals; powder forms, need shaping)	High moment density (Gd^{3+}); large ΔS per volume; chemically stable, mechanically robust single crystals; good for 4 K$\rightarrow$0.4 K stage; huge cooling capacity; good thermal transport.	Limited base temperature (often $>$ 0.3 K) due to long/short range magnetic ordering; hysteresis near ordering; requires high fields ($>$ 4 T) and loses effectiveness $<$ 0.8 K.
Structurally disordered ceramics (e.g. $Gd_{9.33}[SiO_4]_6O_2$, Yb-doped $GdLiF_4$)	$<$ 1 K (no sharp transition)	High (broadly distributed)	Moderate to low (glass-like phonon transport)	Tunable disorder, suppressed ordering to 50 mK; broad Schottky-like heat capacity over 0.1–1 K yields wide operating range; no latent heat losses (continuous magnetization); mechanically hard.	Risk of spin-glass dynamics (slow relaxation); lower thermal conductivity than ordered crystals; internal random fields set a low base-T floor.
Frustrated quantum magnets (e.g. Gd_7 clusters, Yb^{3+}/Gd^{3+}-borates)	$<$ 1 K (order strongly suppressed)	Medium/high (comparable to dense magnets)	Moderate to low (single crystals; powder forms, need shaping)	Reversible cooling with steep isentropes near saturation; large entropy at ultra-low T via degeneracy; field-enhanced cooling (Grüneisen).	Complex synthesis; often powders (high contact resistance), require careful thermal design; dipolar limits at milli-Kelvin regime.
Heavy fermions/ Quantum critical systems (e.g. $YbCu_4Ni$, $YbCo_2Zn_{20}$)	$<$ 0.5 K to $\sim$ 10 mK (tunable to $\sim$ 0 K)	Medium (typically $J = 1/2$ Yb^{3+}/Ce^{3+}, electronic + spin)	High to low (metallic thermal transport; cracked metal pieces, powder forms)	High $\partial T/\partial B$ near QCP; achieved cooling from $\sim$ 2 K to $<$ 50 mK; good for rapid cycling and high cooling power; good thermal conductivity.	Eddy current heating; reduced magnetic entropy (Kondo screening); need to avoid compounds with field-induced phase transitions; expensive materials.

Despite impressive laboratory demonstrations, the transition from fundamental research to widespread deployment faces intrinsic material challenges. Materials synthesis and long-term operational stability represent a primary concern: many quantum-functional refrigerants require precise control of composition, defect structure, and processing conditions to achieve the target disordered or critical states. For instance, the highly frustrated quantum spin liquids and quantum-critical heavy-fermion alloys, while scientifically compelling, often demand stringent synthesis conditions, yield limited sample volumes, and show batch-to-batch variability that complicates scale-up and standardization. Such materials may show structural evolution and performance drift after repeated thermal cycling, requiring robust protocols to ensure reliable operation over hundreds of ADR cycles.

A second fundamental bottleneck arises from the thermal transport dilemma. For the emerging ceramic or polycrystalline quantum materials, the limiting factor is often not the intrinsic thermal conductivity κ, but the inter-granular and refrigerant-to-bus thermal contact resistance (Kapitza resistance). Unlike hydrated salts which can be re-crystallized onto metal wires, chemically stable ceramics are hard to integrate. One promising avenue involves composite architectures that embed metallic thermal-conduction networks within porous magnetic frameworks, though such designs require complex nanofabrication and interfacial engineering with no mature solutions currently available.

Nevertheless, materials innovation remains the key driver of ADR performance advancement. Looking forward, continued discoveries in low-temperature magnetism will produce stronger, broader-range, and more reversible magnetocaloric effects across the entire sub-4 K regime. A key design principle is temperature-stratified customization: matching each refrigerant's magnetic entropy profile (magnitude and temperature distribution), thermal conductivity, and mechanical strength to the functional demands of specific ADR stages.

1–4 K precooling stage Engineering materials with multiple magnetic sublattices showing anisotropic ferro- or ferri-

magnetic interactions can generate abrupt entropy changes under modest field variations slightly above the ordering temperature. Such compounds, exemplified by rare-earth transition-metal intermetallics and complex oxides, deliver large ΔS under relatively low applied fields (approximately 2–4 T), enhancing primary-stage cooling power and reducing cycle durations.

0.1–1 K main cooling stage Precise control of crystal-field splitting, magnetic exchange topology, and geometric frustration through chemical substitution and structural modulation enables fine-tuning of refrigerant properties. The objective is to further suppress magnetic ordering temperatures while preserving high magnetic moment density and broad C/T plateaus spanning approximately 0.05–1 K. Promising candidates are frustrated or structurally disordered rare-earth compounds. Exploiting exotic collective states, such as quantum spin liquids, engineered spin-glass phases, and disorder-stabilized paramagnetic regimes, offers pathways to refrigerants combining large entropy capacity with tunable thermal conductivity.

$<$ 0.1 K electronic cooling stage Fully leveraging quantum-critical materials, such as heavy-fermion metals near magnetic QCPs and insulating frustrated magnets at field-induced criticality, exploiting divergent Grüneisen parameters for quantum-enhanced refrigeration. These mechanisms have demonstrated experimental viability in achieving base temperatures well below 100 mK with reasonable field magnitudes (4–9 T), offering practical alternatives to conventional ^{3}He-based dilution refrigeration in resource-constrained environments.

For temperatures significantly below 1 mK, nuclear adiabatic demagnetization (NDR) using materials like Cu or $PrNi_5$ remains the irreplaceable standard due to their ultra-small nuclear magnetic moments. However, in the intermediate 1–100 mK regime, the quantum electronic refrigerants reviewed here offer a compact, high-cooling-power alternative to complex nuclear stages.

As novel quantum magnetic states continue to be discovered and translated into functional refrigerants, ADR technology will provide increasingly powerful cryogenic infrastructure for exploring matter and the universe under extreme conditions. The ongoing evolution from weakly interacting paramagnets to quantum-enhanced many-body systems represents not merely incremental performance gains but a fundamental shift in ultra-low temperature refrigeration. This transformation leverages the richness of condensed-matter quantum phenomena, e.g. frustration, criticality, and correlated disorder, to overcome limitations inherent to classical single-ion refrigerants. The trajectory of ADR development thus mirrors broader trends in quantum materials science, from phenomenological exploitation of simple quantum states toward the rational design of complex collective behaviors tailored for specific technological functions. This evolution will continue expanding the frontiers of cryogenic science and engineering, enabling transformative advances in quantum computing, astrophysical instrumentation, and fundamental physics research that probe the deepest mysteries of nature at the coldest accessible temperatures.

Acknowledgements

This work was supported by the National Key R&D Program of China (Grant No. 2021YFA1400300), the Guangdong Basic and Applied Basic Research Foundation (Grant No. 2022A1515111009), and the National Natural Science Foundation of China (Grant Nos. 12425403, 12261131499, and 52273298).

References

[1] Chen Z, Shen J, Zhao Y N, Zheng W, Yang L, Lu Y, Liu J and Li Z 2025 *Appl. Therm. Eng.* **265** 125562
[2] Shirron P J 2014 *Cryogenics* **62** 130
[3] Shirron P J, Kimball M O, Ottens R S, James B L, Canavan E R, DiPirro M J, Bialas T A, Sneiderman G A, Kilbourne C A, Porter F S, Kelley R L, Barnstable K R, Fujimoto R, Takei Y and Yoshida S 2025 *J. Astron. Telesc. Inst.* **11** 042015
[4] Jiang C, Li C, Jin H and Cui W 2023 *Sci. Bull.* **68** 2709
[5] Zu H, Dai W and De Waele A 2022 *Cryogenics* **121** 103390
[6] Debye P 1926 *Ann. Phys.* **386** 1154
[7] Giauque W 1927 *J. Am. Chem. Soc.* **49** 1864
[8] Giauque W and MacDougall D 1933 *Phys. Rev.* **43** 768
[9] Khramov Y A 1985 *Sov. J. Low Temp. Phys.* **11** 672
[10] De Haas W, Wiersma E and Kramers H 1934 *Physica* **1** 1
[11] Heer C, Barnes C and Daunt J 1953 *Phys. Rev.* **91** 412
[12] Heer C, Barnes C and Daunt J 1954 *Rev. Sci. Instrum.* **25** 1088
[13] Zimmerman J, McNutt J and Bohm H 1962 *Cryogenics* **2** 153
[14] Rosenblum S, Sheinberg H, and Steyert W 1976 *Cryogenics* **16** 245
[15] Wikus P, Canavan E, Heine S T, Matsumoto K and Numazawa T 2014 *Cryogenics* **62** 150
[16] Treu T, Klinger M, Oefele N, Telang P, Jesche A and Gegenwart P 2024 *J. Phys.: Condens. Matter* **37** 013001
[17] Xu Q F, Wu R T, Long L S and Zheng L S 2025 *Acc. Chem. Res.* **58** 2898
[18] Barclay J A, Rosebblum S S and Steyert W A 1976 *Cryogenics* **16** 539
[19] Fisher R, Hornung E, Brodale G and Giauque W 1973 *J. Chem. Phys.* **58** 5584
[20] Vilches O and Wheatley J 1966 *Rev. Sci. Instrum.* **37** 819
[21] Kleinhans M, Eibensteiner K, Leiner J C, Spallek J, Regnat A and Pfleiderer C 2023 *Phys. Rev. Appl.* **19** 014038
[22] Barclay J A 1988 *Adv. Cryog. Eng.* **33** 719
[23] Brasiliano D A P, Duval J M, Marin C, Bichaud E, Brison J P, Zhitomirsky M and Luchier N 2020 *Cryogenics* **105** 103002
[24] McMichael R D, Ritter J J and Shull R D 1993 *J. Appl. Phys.* **73** 6946
[25] Numazawa T, Kamiya K, Shirron P, DiPirro M and Matsumoto K 2006 *AIP Conf. Proc.* **850** 1579
[26] Morozov O A, Korableva S L, Nurtdinova L A, Kyashkin V M, Popov P A, Klimovitskii A E, Pudovkin M S and Semashko V V 2023 *Opt. Mater.* **137** 113490
[27] DiPirro M, Canavan E, Shirron P and Tuttle J 2004 *Cryogenics* **44** 559
[28] Yang Z W, Zhang J, Lu D, Zhang X, Zhao H, Cui H, Zeng Y J and Long Y 2023 *Inorg. Chem.* **62** 5282
[29] Yang Z, Ge J Y, Ruan S, Cui H and Zeng Y J 2021 *J. Mater. Chem. C* **9** 6754
[30] Yang Z, Zhang H, Bai M , Li W, Huang S, Ruan S and Zeng Y J 2020 *J. Mater. Chem. C* **8** 11866
[31] Wang B, Liu X, Hu F, Wang J T, Xiang Y, Sun P, Wang J, Sun J, Zhao T and Mo Z 2024 *J. Am. Chem. Soc.* **146** 35016
[32] Wang Y, Xiang J, Zhang L, Gong J, Li W, Mo Z and Shen J 2024 *J. Am. Chem. Soc.* **146** 3315

[33] Xu Q, Liu B, Ye M, Zhuang G, Long L and Zheng L 2022 *J. Am. Chem. Soc.* **144** 13787

[34] Xu P, Ma Z, Wang P, Wang H and Li L 2021 *Mater. Today Phys.* **20** 100470

[35] Palacios E, Rodríguez-Velamazán J A, Evangelisti M, McIntyre G J, Lorusso G, Visser D, De Jongh L and Boatner L A 2014 *Phys. Rev. B* **90** 214423

[36] Song Z M, Zhao N, Ge H, Li T T, Yang J, Wang L, Fu Y, Zhang Y Z, Wang S M, Mei J W, He H, Guo S, Wu L S and Sheng J M 2023 *Phys. Rev. B* **107** 125126

[37] Yang Z, Qin S, Ye X, Liu Z, Guo Y, Cui H, Ge J Y, Li H, Long Y and Zeng Y J 2022 *Sci. China: Phys., Mech. Astron.* **65** 247011

[38] Wang Y, Xiang J, Zhang L, Gong J, Li W, Mo Z and Shen J 2024 *J. Am. Chem. Soc.* **146** 3315

[39] Zhang Y, Hao W, Lin J, Li H Fand Li L 2024 *Acta Mater.* **272** 119946

[40] Yang Z W, Qin S, Zhang J, Lu D, Zhao H, Kang C, Cui H, Long Y and Zeng Y J 2022 *Mater. Today Phys.* **27** 100810

[41] Song F Y, Liu X Y, Dong C, Zhou J, Shi X L, Han Y Y, Ling L S, Ren H F, Yuan S L, Wang S, Xiang J S, Sun P J and Tian Z M 2025 *Chin. Phys. Lett.* **42** 120706

[42] Zhang Y, Li A, Hao W, Li H F and Li L 2025 *Acta Mater.* **292** 121033

[43] Zhang Y, Na Y, Hao W, Gottschall T and Li L 2024 *Adv. Funct. Mater.* **34** 2409061

[44] Yang Z W, Zhang J, Liu B, Zhang X, Lu D, Zhao H, Pi M, Cui H, Zeng Y J, Pan Z, Shen Y, Li S and Long Y 2024 *Adv. Sci* **11** 2306842

[45] Xu Q F, Zhao P, Chen M T, Wu R T, Dai W, Long L S and Zheng L S 2025 *Adv. Mater.* **37** 2414226

[46] Zhitomirsky M 2003 *Phys. Rev. B* **67** 104421

[47] Koskelo E C, Mukherjee P, Liu C, Sackville Hamilton A C, Ong H S, Castelnovo C, Zhitomirsky M and Dutton S E 2023 *PRX Energy* **2** 033005

[48] Manvell A S, Dunstan M A, Gracia D, Hruby J, Kubus M, McPherson J N, Palacios E, Weihe H, Hill S and Schnack J 2025 *J. Am. Chem. Soc.* **147** 7597

[49] Sharples J W, Collison D, McInnes E J L, Schnack J, Palacios E and Evangelisti M 2014 *Nat. Commun.* **5** 5321

[50] Bulled J M, Paddison J A, Wildes A, Lhotel E, Cassidy S J, Pato-DoldÁn B, Gḿez-Aguirre L C, Saines P J and Goodwin A L 2022 *Phys. Rev. Lett.* **128** 177201

[51] Tokiwa Y, Bachus S, Kavita K, Jesche A, Tsirlin A A and Gegenwart P 2021 *Commun. Mater.* **2** 42

[52] Jesche A, Winterhalter-Stocker N, Hirschberger F, Bellon A, Bachus S, Tokiwa Y, Tsirlin A A and Gegenwart P 2023 *Phys. Rev. B* **107** 104402

[53] Gegenwart P, Si Q and Steglich F 2008 *Nat. Phys.* **4** 186

[54] Shimura Y, Watanabe K, Taniguchi T, Osato K, Yamamoto R, Kusanose Y, Umeo K, Fujita M, Onimaru T and Takabatake T 2022 *J. Appl. Phys.* **131** 013903

[55] Gruner T, Chen J, Jang D, Banda J, Geibel C, Brando M and Grosche F M 2024 *Commun. Mater.* **5** 63

[56] Tokiwa Y, Piening B, Jeevan H S, Bud'ko S L, Canfield P C and Gegenwart P 2016 *Sci. Adv.* **2** e1600835

[57] Wolf B, Tsui Y, Jaiswal-Nagar D, Tutsch U, Honecker A, Remović-Langer K, Hofmann G, Prokofiev A, Assmus W and Donath G 2011 *Proc. Natl. Acad. Sci. USA* **108** 6862